

Session 2P1

Nanostructures and Metamaterials for RF and Optical Applications

Exotic Waves in Chains of Silver Nanospheres	
<i>C. R. Simovski (Helsinki University of Technology, Finland); A. J. Viitanen (Helsinki University of Technology, Finland); S. A. Tretyakov (Helsinki University of Technology, Finland);</i>	550
Light Scattering on 2D Nanostructured Resonant Gratings	
<i>N. V. Ilyin (Institute of Applied Physics, Russia); I. G. Kondratiev (Institute of Applied Physics, Russia); N. V. Sapogova (Institute of Applied Physics, Russia); A. I. Smirnov (Institute of Applied Physics, Russia);</i>	551
New Resonant Elements for Isotropic Magnetic Metamaterials	
<i>J. D. Baena (University of Sevilla, Spain); L. Jelinek (Czech Technical University, Czech Republic); R. Marqués (University of Sevilla, Spain); J. Zehentner (Czech Technical University, Czech Republic);</i>	555
Modified Equivalent Circuit Model of Microwave Filter with LTCC Technique	
<i>Y. L. Qin (Zhejiang University of Technology, China); A. Fang (Zhejiang University of Technology, China); J. Hu (Zhejiang University of Technology, China); W. W. Zhou (Zhejiang University of Technology, China); M. Zhang (Zhejiang University of Technology, China);</i>	556
Design of a Metafilm-composite Dielectric Shielding Structure Using a Genetic Algorithm	
<i>J. Y. Huang (University of Missouri-Rolla, USA); M. Y. Koledintseva (University of Missouri-Rolla, USA); P. C. Ravva (University of Missouri-Rolla, USA); J. L. Drewniak (University of Missouri-Rolla, USA); R. E. DuBroff (University of Missouri-Rolla, USA); B. Archambeault (IBM Co., USA); K. N. Rozanov (Russian Academy of Sciences, Russia);</i>	561
Towards Nano-scales in Photonics	
<i>M. Soljačić (MIT, USA); A. Karalis (MIT, USA); E. Lidorikis (MIT, USA); M. Ibanescu (MIT, USA); L. V. Hau (Harvard University, MIT); J. D. Joannopoulos (MIT, USA);</i>	566
Design and Measurement of a Four-port Device Using Left-handed Metamaterials	
<i>Z. M. Thomas (Massachusetts Institute of Technology, USA); T. M. Grzegorzcyk (Massachusetts Institute of Technology, USA); B.-I. Wu (Massachusetts Institute of Technology, USA); X. D. Chen (Massachusetts Institute of Technology, USA); J. A. Kong (Massachusetts Institute of Technology, USA);</i>	567
Embedded-circuit Meta-materials for Surface Wave Suppression	
<i>H. Mosallaei (Northeastern University, USA);</i>	568
Double Clad Fiber Laser with Frequency Selecting by Double Clad Fiber Bragg Grating	
<i>T. Wu (LongYan University, China); Z.-D. Xue (Fuzhou University, China);</i>	569
Ferroelectric PSTO and Mn: BSTO Thin Films for Wireless Microwave Elements	
<i>Z. Yuan (University of Texas at San Antonio, USA); S. W. Liu (University of Arkansas, USA); C. L. Chen (University of Texas at San Antonio, USA);</i>	570
Chain of Metamaterial Nanospheres as Leaky-wave Nanoantennas at Optical Frequencies	
<i>A. Alù (University of Pennsylvania, USA); N. Engheta (University of Pennsylvania, USA);</i>	571
Epsilon-near-zero (ENZ) Materials as Insulators for Nanocircuit Elements	
<i>M. G. Silveirinha (University of Pennsylvania, USA); N. Engheta (University of Pennsylvania, USA); ..</i>	572
Leaky-mode Resonance Properties of Periodic Lattices and Their Applications	
<i>R. Magnusson (University of Connecticut, USA); Y. Ding (University of Connecticut, USA);</i>	573
Slow-than-light Transportation of Microwave through Subwavelength Fractal Slots	
<i>B. Hou (The Hong Kong University of Science and Technology, China); W. J. Wen (The Hong Kong University of Science and Technology, China); P. Sheng (The Hong Kong University of Science and Technology, China);</i>	574

Exotic Waves in Chains of Silver Nanospheres

C. R. Simovski^{1,2}, A. J. Viitanen¹, and S. A. Tretyakov¹

¹Helsinki University of Technology, Finland

²St. Petersburg Institute of Fine Mechanics and Optics, Russia

A transversal mode with zero group velocity and non-zero phase velocity that can exist in chains of silver nanospheres in the optical frequency range is theoretically studied. In such chains at a certain special frequency a monochromatic source excites the standing wave in an infinite chain, and as a result we obtain an optical resonator without spatial bounds. It is shown that the external source radiating a narrow-band non-monochromatic signal excites in the chain a mixture of standing and slowly traveling waves. The standing wave component (named as *resonator mode*) is strongly dominating. The physical reason of such a regime is an unusual distribution of power flux over the cross section of the chain. The study shows that the axial Poynting vector is negative on the chain axis and changes its sign at a certain distance ρ_0 from it, so that the total energy flux of the pulse turns out to be positive. The most part of the pulse energy propagating along the chain in the positive direction returns back inside a narrow spatial channel centered at the chain axis. Since the chain period for such a regime is obviously small compared to the wavelength in free space, the energy is concentrated in a subwavelength spatial region. Besides of very efficient slow-wave lines these chains can be also used for subwavelength localization of the light energy. The possible application for obtaining subwavelength images is discussed.

Next, chains with alternating spheres that differ by diameters (or, perhaps, covered with dielectric material) — two-phase chains — are studied. A small change of polarizabilities of spheres in these two sub-arrays results in new interesting properties. One of them is a significant broadening of the propagation band. For the case of the longitudinal polarization of spheres there is a narrow stop-band at the center of the band of eigenfrequencies, and one can obtain a high-quality band-stop filter. A single-phase chain of silver nanospheres can be considered as a filter with a narrow pass-band whose remarkable property is the subwavelength localization of the field. Two-phase chains behave as band-stop filters, also with subwavelength localization of the field. Other interesting features of this structure are also discussed.

Light Scattering on 2D Nanostructured Resonant Gratings

N. V. Ilyin, I. G. Kondratiev, N. V. Sapogova, and A. I. Smirnov
 Institute of Applied Physics, Russia

Abstract—This paper studies nanostructured gratings made up by silver nanoparticles embedded in the dielectric, which are capable of maintaining quasi-static modes. The special emphasis is devoted to following specified types of gratings: row of periodical cylinders and square grating of spheres. The problem of a diffraction of a plane electromagnetic wave on such structures has been solved within the dipolar-interaction approximation. The frequency dependences of the refraction and absorption coefficients on the grating parameters have been obtained, analyzed and compared.

1. Introduction

Recently, a significant success has been achieved in the areas related to creation of metamaterials based on resonance metal elements, specifically, films with embedded metal nanoparticles [1–3] that are capable of sustaining high-Q-factor quasi-static modes. At the resonance frequency, the scattering cross-section of such particles exceeds their geometric sizes significantly, which yields a number of new collective optical properties when they join up in nanostructures. The most preferable, in terms of practical applications (both from the standpoint of their chemical stability and resonance characteristics), are the nanoparticles of silver and gold. The coherent effects of light scattering on plane gratings formed by cylindrical and spherical nanometer silver objects have been analyzed.

2. Diffraction on a Periodical Structures

This work studies the diffraction of a plane P-polarized wave with the form:

$$\begin{aligned} H_y &= H_o \exp(-i\omega t - ik_o \cos\varphi z - ik_o \sin\varphi x) \\ E_x &= -E_o \cos\varphi \exp(-i\omega t - ik_o \cos\varphi z - ik_o \sin\varphi x) \\ E_z &= -E_o \sin\varphi \exp(-i\omega t - ik_o \cos\varphi z - ik_o \sin\varphi x) \end{aligned} \tag{1}$$

that falls from the vacuum onto a plane grating formed by silver nanostructures (see Figure 1). Two simplest and at the same time, evidently, basic configurations of the grating are considered: the first (unidimensional) is a periodic row of cylinders with their axes lying in the plane $z = 0$ and oriented along the y -axis (see Figure 1a), and the second (two-dimensional) is a periodic (both along x and y) square grating of spheres with their centres in the plane $z = 0$ (see Figure 1b).

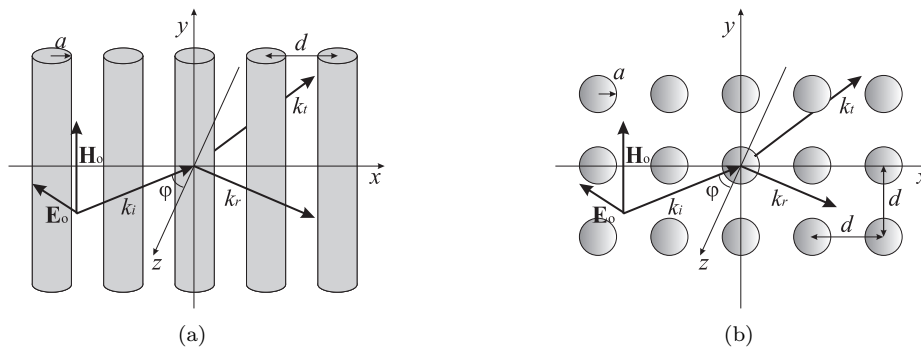


Figure 1: Configurations of considering gratings.

Let us assume, for the sake of simplicity, that the dielectric permittivity of the substrate, which the grating is mounted on, is close to unity, such that the environment is actually vacuum everywhere. Let the radii of the cylinders and the spheres are small as compared with the length of the incident wave λ ($a \ll \lambda$). Then the field scattered by these structural elements is the field of a linear dipole with its dipole momentum (per length unit) $\mathbf{P}_{cyl} = \alpha_{cyl} \mathbf{E}_D$ for the cylinder, and the field of a point dipole with its dipole momentum $\mathbf{P}_{sph} = \alpha_{sph} \mathbf{E}_D$ for the sphere, where \mathbf{E}_D is the effective field. When radiation losses are neglected, the polarizability coefficients look as follows (see Figure 2):

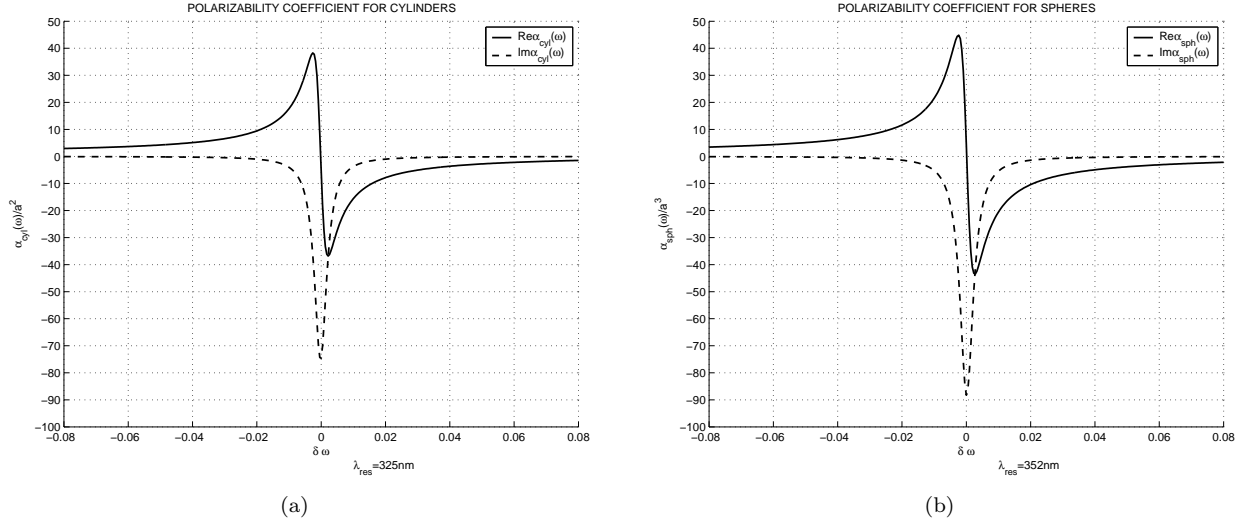


Figure 2: Polarizability coefficients of considering elements as a function of relative frequency shift $\delta\omega = \frac{\omega - \omega_{res}}{\omega_{res}}$ ($\lambda_{res} = 325nm$ for cylinders, $\lambda_{res} = 352nm$ for spheres).

$$\alpha_{cyl} = \frac{\varepsilon(\omega) - 1}{\varepsilon(\omega) + 1} a^2 \qquad \alpha_{sph} = \frac{\varepsilon(\omega) - 1}{\varepsilon(\omega) + 2} a^3 \quad (2)$$

Here $\varepsilon(\omega)$ is the dielectric permittivity of the object. For silver, which is interest for us, it is described, in the range $\lambda \sim 300 - 500nm$, with good accuracy as [4]:

$$\varepsilon(\omega) = \varepsilon_\infty - \frac{\omega_p^2}{\omega(\omega - i\gamma)} \quad (3)$$

where $\varepsilon_\infty = 4.7$, $\omega_p = 1.38 \cdot 10^{16} s^{-1}$, $\gamma = 2.7 \cdot 10^{13} s^{-1}$.

The effective field is the sum of the incident field and the fields of all other dipoles at the location of some segregated dipole in its absence. We propose that the following procedure should be used to find that field, which is somewhat different from the traditional procedure and, in our opinion, seems to be convenient. Taking into account that a polarized medium can be described by means of polarization currents $\mathbf{J} = \frac{\partial \mathbf{P}}{\partial t} = -i\omega \mathbf{P}$, let us pass over from dipoles to currents. The density of such currents is represented as:

$$\begin{aligned} \mathbf{J}_{cyl}(x) &= -i\omega \alpha_{cyl}(\omega) \mathbf{E}_D^{cyl} \delta(z) \sum_{n=-\infty}^{+\infty} \delta(x - nd) \\ \mathbf{J}_{sph}(x, y) &= -i\omega \alpha_{sph}(\omega) \mathbf{E}_D^{sph} \delta(z) \sum_{n=-\infty}^{+\infty} \sum_{m=-\infty}^{+\infty} \delta(x - nd) \delta(y - md) \end{aligned} \quad (4)$$

where $\delta(\cdot)$ is the Dirac δ function.

Then, from the shown system of discrete currents, using the Poisson formula [5] we pass over to continuous surface dummy currents of spatial harmonics:

$$\begin{aligned} \mathbf{J}_{cyl}(x) &= -i\omega \alpha_{cyl}(\omega) \mathbf{E}_D^{cyl} \frac{\delta(z)}{d} \sum_{n=-\infty}^{+\infty} \exp(i \frac{2\pi}{d} nx) \\ \mathbf{J}_{sph}(x, y) &= -i\omega \alpha_{sph}(\omega) \mathbf{E}_D^{sph} \frac{\delta(z)}{d^2} \sum_{n=-\infty}^{+\infty} \sum_{m=-\infty}^{+\infty} \exp(i \frac{2\pi}{d} nx) \exp(i \frac{2\pi}{d} my) \end{aligned} \quad (5)$$

Finding the field of the individual spatial harmonic is elementary for the tangential component of the current, and somewhat more difficult for the normal one. Note that the normal component of the electric field is actually equivalent to the tangential of the magnetic current. The effective field is further obtained by subtracting the field of the segregated dipole situated, e. g., at the origin of coordinates. Representing the latter as an integral over the same harmonics, we obtain finally the following self-consistent expressions:

$$\mathbf{E}_D^{cyl}(0) = \mathbf{E}_o(x = z = 0) + \sum_{n=-\infty}^{+\infty} \tilde{\mathbf{E}}(\chi_x = \frac{2\pi}{d}n) - \frac{d}{2\pi} \int_{-\infty}^{+\infty} d\chi_x \tilde{\mathbf{E}}(\chi_x)$$

$$\mathbf{E}_D^{sph}(0,0) = \mathbf{E}_o(x = z = 0) + \sum_{n=-\infty}^{+\infty} \sum_{m=-\infty}^{+\infty} \tilde{\mathbf{E}}(\chi_x = \frac{2\pi}{d}n, \chi_y = \frac{2\pi}{d}m) - \frac{d^2}{4\pi^2} \int_{-\infty}^{+\infty} \int_{-\infty}^{+\infty} d\chi_x d\chi_y \tilde{\mathbf{E}}(\chi_x, \chi_y) \quad (6)$$

from which the effective field is extracted as a function of the incident field. It should be noted that the second and third term in formula (6) have singularities at zero, which are mutually compensated. This should be taken into account when performing numerical calculations.

Granted that the effective field is known, it is possible to solve the set diffraction problem.

3. Results and Discussion

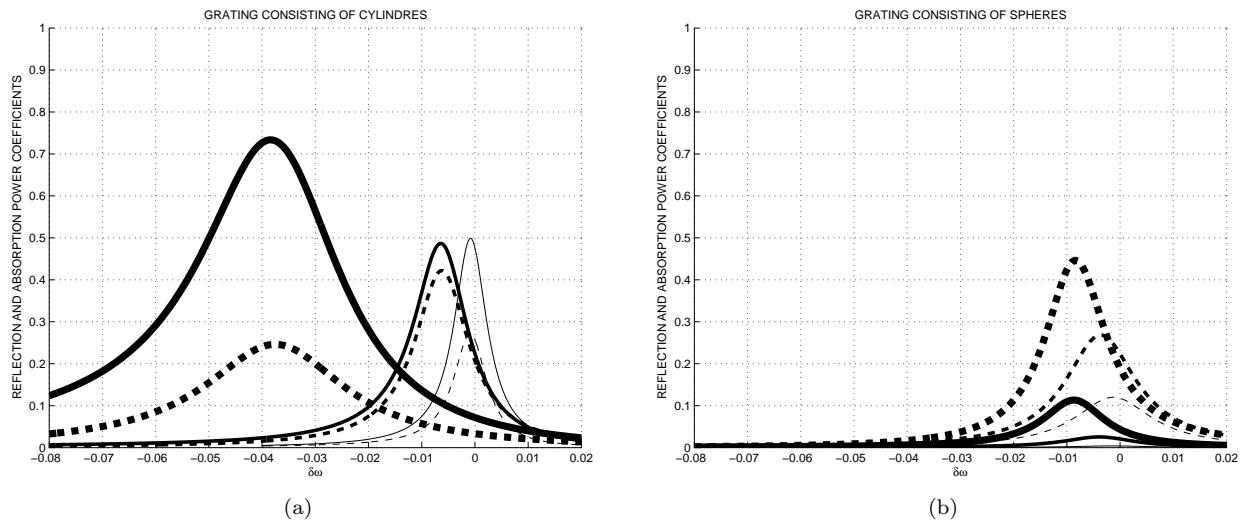


Figure 3: Reflection (firm line) and absorption (dash line) power coefficients of considered gratings as a function of relative frequency shift $\delta\omega = \frac{\omega - \omega_{res}}{\omega_{res}}$ for various periods d of gratings ($a/d = 0.2$ —blue line, $a/d = 0.1$ —green line, $a/d = 0.05$ —red line). The normal incidence case ($\varphi = 0$).

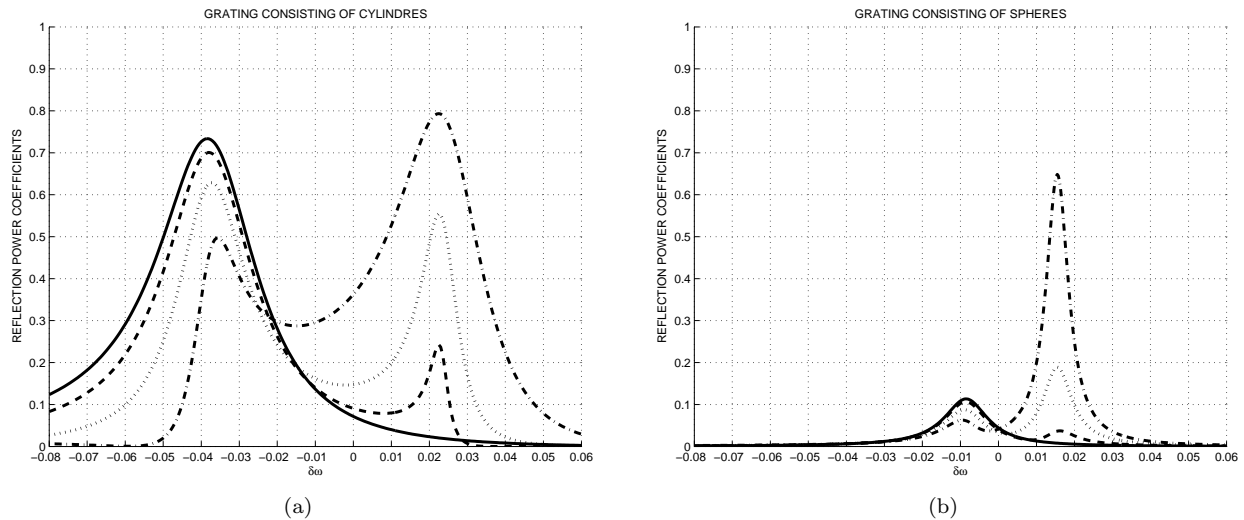


Figure 4: Reflection power coefficients of considered gratings as a function of relative frequency shift $\delta\omega = \frac{\omega - \omega_{res}}{\omega_{res}}$ for various incidence angles ($\varphi = 0^\circ$ —red line, $\varphi = 30^\circ$ —green line, $\varphi = 50^\circ$ —blue line, $\varphi = 70^\circ$ —black line). Relation $a/d = 0.2$ is fixed.

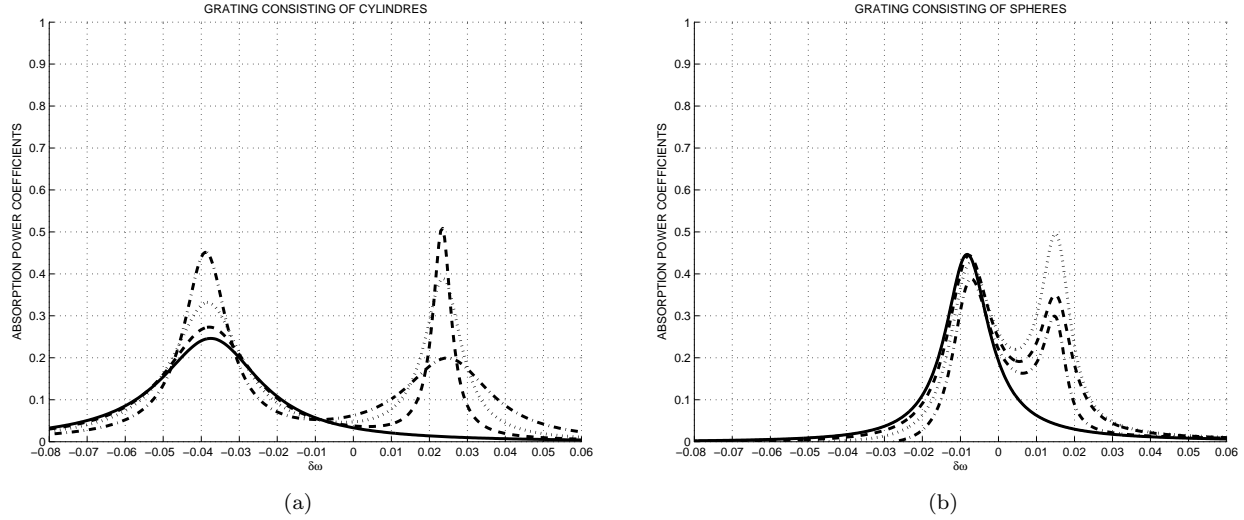


Figure 5: Absorption power coefficients of considered gratings as a function of relative frequency shift $\delta\omega = \frac{\omega - \omega_{res}}{\omega_{res}}$ for various incidence angles ($\varphi = 0^\circ$ —red line, $\varphi = 30^\circ$ —green line, $\varphi = 50^\circ$ —blue line, $\varphi = 70^\circ$ —black line). Relation $a/d = 0.2$ is fixed.

Further the results of the numerical calculations based on the formulas (6) are presented and discussed. Reflection and absorption power coefficients as a function of relative frequency shift $\delta\omega = \frac{\omega - \omega_{res}}{\omega_{res}}$ for various grating parameters are shown in Figures 3, 4, 5. All results are given for the fixed parameter $k_{res}a = \frac{\omega_{res}}{c}a = 0.08$. Thus, the radius of cylinders a is equal $4.1nm$ and the radius of spheres a is equal $4.5nm$. The left-hand parts of figures respond a case of the grating from cylinders, and right parts—to a case of the grating from spheres. Comparison allows to present common features and distinctivenesses.

Figure 3 convincingly shows effect of coherent interaction of separate elements at their converging. The peak value of reflection coefficients for the grating from spheres is noticeably less than for the grating from cylinders. It is stipulated by essential difference in filling factors ($f_{cyl}/f_{sph} = 4a/3d$). Different shift of frequencies, at which the maxima of reflection coefficient for considered gratings is attained, is determined, apparently, various interactions of linear dipoles and point dipoles.

In case of oblique incidence (see Figure 4) with increase of an incidence angle, one more peak occurs and gradually grows. It is stipulated by coherent interaction dipoles oriented along the z -axis.

4. Conclusion

A two-dimensional problem of plane electromagnetic wave diffraction on a gratings consisting of resonance elements is solved in dipole-interaction approximation. A novel method of obtaining effective field expression is proposed. Reflection and absorption coefficients are found for various compositions of gratings parameters.

REFERENCES

1. Malynych, S., I. Lurinov, and G. Chumanov, *J. Phys. Chem.*, No. 106, 1280–1282, 2002.
2. Malynych, S., H. Robuck, and G. Chumanov, *Nano Letters*, No. 1, 647–649, 2001.
3. Pinna, N., M. Maillard, A. Courty, V. Russier, and M. P. Pileni, *Phys. Ref. B*, 045415, 2002.
4. Huebner, R. H., E. T. Arakawa, R. A. McRae, and R. N. Hamm, *J. Opt. Soc. Am.*, Vol. 54, 1434, 1963.
5. Collin, R., *Field Theory of Guided Waves*, IEEE Press, Piscataway, NJ, 1990.

New Resonant Elements for Isotropic Magnetic Metamaterials

J. D. Baena¹, L. Jelinek², R. Marqués¹, and J. Zehentner²

¹University of Sevilla, Spain

²Czech Technical University, Czech Republic

In 1999 Split Ring Resonator (SRR), as a unit cell of negative permeability media, was first introduced by Pendry [1]. Afterwards, Smith et al., [2] analyzed an array of wires and SRRs obtaining an artificial medium with simultaneously negative permittivity and permeability. This was the first realization of a left-handed medium which was theoretically studied by Veselago [3] several decades ago. However, this and subsequent realizations were highly anisotropic. A first attempt towards the design of isotropic magnetic metamaterials was made by Gay-Balmaz and Oliver Martin [4], who obtained a 2D isotropic SRR. The SRR is not the unique candidate for artificial quasi-isotropic medium, as was demonstrated by using Ω particles in [5]. More recently, an SRR based proposal for isotropic magnetic metamaterial design has been presented [6].

The main aim of this work is to design particles from which an isotropic media can be made. Really, no material composed by periodical arrangement of unit cells can be fully isotropic. However, in many cases the behavior of such system can be characterized by second order tensors (e.g., the electric, magnetic or magneto-electric polarizability tensors), without considering tensors of higher orders. The cubic structures of Figs. 1 and 2 show the group of symmetry of the cube, thus being candidates for fully isotropic magnetic metamaterials [6]. In addition, it can be shown that the sub-group generated by the four operations (\mathbf{I} , $-\mathbf{I}$, $\mathbf{C}_{4x}\mathbf{C}_{4y}$, $\mathbf{C}_{4y}\mathbf{C}_{4x}$) also provides isotropic tensors. An example of an isotropic resonator invariant by this group of symmetry (in fact a modification of a previous proposal [7]) is shown in Fig. 3. A modification of Fig. 2 which substitutes the four gaps broadside-coupled SRR (BCSRR) by a simpler two-gaps BC-SRR is also invariant by the aforementioned symmetry group. Finally, the elimination of the inversion ($-\mathbf{I}$) operation may lead to bi-isotropic magnetic media.



Figure 1.

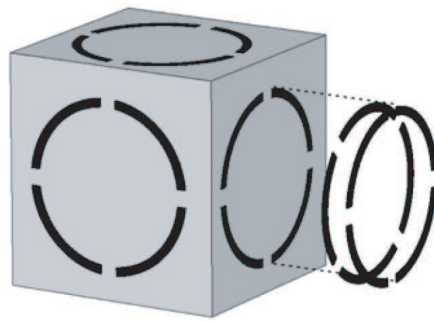


Figure 2.

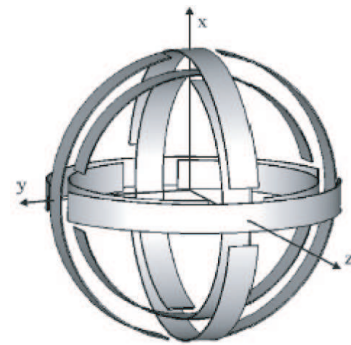


Figure 3.

REFERENCES

1. Pendry, J. B., et al., *IEEE Trans. on MTT*, Vol. 47, 2075, 1999.
2. Smith, D., et al., *Phys. Rev. Lett.*, Vol. 84, 4184, 2000.
3. Veselago, V., *Soviet Physics USPEKHI*, Vol. 10, 509, 1968.
4. Gay-Balmaz, P. and O. J. F. Martin, *Appl. Phys. Lett.*, Vol. 81, 939, 2002.
5. Simovski, C. R. and S. He, *Phys. Lett. A*, Vol. 311, 254, 2003.
6. Koschny, Th., L. Zhang, and C. M. Soukoulis, *Phys. Rev. B*, Vol. 71, 121103(R), 2005.
7. Marqués, R., J. D. Baena, J. Martel, F. Medina, F. Falcone, M. Sorolla, and F. Martin, *Proc. of the ICEAA'03*, 439, Pisa, Italy, Sept. 2003.

Modified Equivalent Circuit Model of Microwave Filter with LTCC Technique

Y. L. Qin, A. Fang, J. Hu, W. W. Zhou, and M. Zhang
Zhejiang University of Technology, China

Abstract—Because microwave products in the consumer electronics market are continuous developing, device and component manufacturers have to seek new advanced integration, packaging and interconnection technologies, as size, cost and performance are critical factors for the success of a microwave product.

One of the most promising integration technologies is the multilayer low temperature co-fired ceramic technology (LTCC). In this technology, passive components, such as inductors, capacitors and filters, are integrated into multilayer LTCC substrate. The purpose of this paper is to address the special method that should be considered for designing LTCC microwave filter. It is given how to get equivalent circuit about multilayer ceramic microwave filter that is striplines configuration or LC configuration, especially, modified equivalent circuit model is proposed, where the relation between the lumped parameters and physical dimension of LTCC microwave filter is discussed. The capacitance and inductance matrix of LTCC microwave filter is obtained using the fast multipole method. Finally, two microwave filters are designed by the novel design method of field-circuit and HFSS. The novel design method of field-circuit is more efficient, therefore, the designing time can be shortened.

1. Introduction

Low-temperature-cofired ceramics (LTCC) for microwave applications represent a key position in the development of future electronic products in a high frequency application for IC packaging radar, antennas and wireless technologies. The integration of passive components in LTCC is, therefore, particularly interesting in multilayers technology. Integration of passive devices in wireless application corresponds to the trend of mobilization and miniaturization with high electrical performance using conductive electrode materials such as gold, silver and copper. Several kinds of multilayer microwave devices have been developed, and some design methods and fabrication procedures reported [1–4]. Hence, they can be easily incorporated in the design of a variety of RF components such as passive components, voltage controlled oscillators (VCO_s), power amplifiers (PA_s), and mixers.

Among various passive components, people usually pay the most attention to the filter. Now a lumped-element RF filter can be implemented in a stacked structure. Engineers usually use HFSS, which is a software employed by Ansoft used for high frequency E/M simulation, to design these passive components. One side, HFSS is an advanced simulation software, which can accurately calculate the E/M fields with every engaged point in the component. So its result is convictive. On the other side, HFSS is not very effectively because of long time waste depending on the capability of your computer and the simulation precision you want. This paper introduces the designing of fast multipole method for the passive filter. It is shown more effective than the HFSS by experiment proof-testing.

2. Getting Capacitance and Inductance Matrix Using the Fast Multipole Method (FMM)

Figure 1 shows there are M conductors between two grounds. $\therefore Q_n = \sum_{m=1}^M C_{n,m} V_m$, where Q_n is the quantity of charge of conductor n and V_m is the electric potential of conductor m . $C_{n,m}$ represents the capacitance between conductor n and conductor m when the electric potential of conductor m is V_m and the electric potential of conductor n is 0.

Provided that S_n , $\rho_n(r')$ are, respectively, the superficial area and surface charge density of conductor n , quantities of electric charge Q_n of conductor n can be given as:

$$Q_n = \int_{S_n} \rho_n(r') dS \quad (1)$$

For every point on the conductor surface, the electric potential of the point can be driven by considering the

image charges, we have

$$\Psi(r) = \frac{1}{4\pi\epsilon_r\epsilon_0} \left[\sum_{n=1}^M \int_{S_n} \frac{\rho_n(r')}{|r-r'|} dS + \sum_{i=1}^{\infty} \sum_{n=1}^M \int_{S_n^i} \frac{\rho'_{n,i}(r')}{|r-r'_{n,i}|} dS \right]; r \in S_m, m = 1, 2, \dots, M \quad (2)$$

where $\rho'_{n,i}(r')$ represents the i -th mirror of $\rho'_n(r')$, S_n^i represents the superficies of $\rho'_n(r')$.

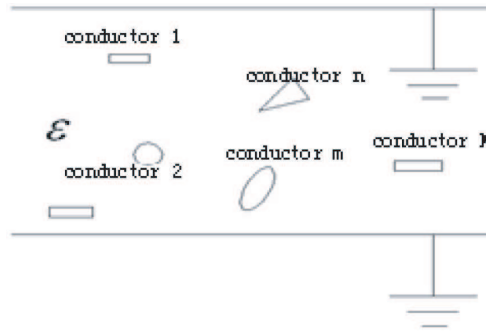


Figure 1: Multi-conductor system in medium between two grounds.

Using moments method we can divide the superficies of the conductor to N pieces, provided that the charge on every piece is uniform:

$$\Psi_l(r_l) = \frac{1}{4\pi\epsilon_r\epsilon_0} \left[\sum_{k=1}^N \int_{T_k} \frac{\rho_l(r')}{|r_l-r'|} dS + \sum_{i=1}^{\infty} \sum_{k=1}^N \int_{T_k^i} \frac{\rho'_{l,i}(r')}{|r_l-r'_{l,i}|} dS \right]; r \in T_k, k = 1, 2, \dots, N \quad (3)$$

The capacitance matrix can be formed by the above sets of equations:

$$[C]_{n,m} = \begin{bmatrix} C_{1,1} & C_{1,2} & \dots & \dots & C_{1,M-1} & C_{1,M} \\ C_{2,1} & C_{2,2} & \dots & \dots & C_{2,M-1} & C_{2,M} \\ \dots & \dots & \dots & \dots & \dots & \dots \\ \dots & \dots & \dots & \dots & \dots & \dots \\ C_{M-1,1} & C_{M-1,2} & \dots & \dots & C_{M-1,M-1} & C_{M-1,M} \\ C_{M,1} & C_{M,2} & \dots & \dots & C_{M,M-1} & C_{M,M} \end{bmatrix} \quad (4)$$

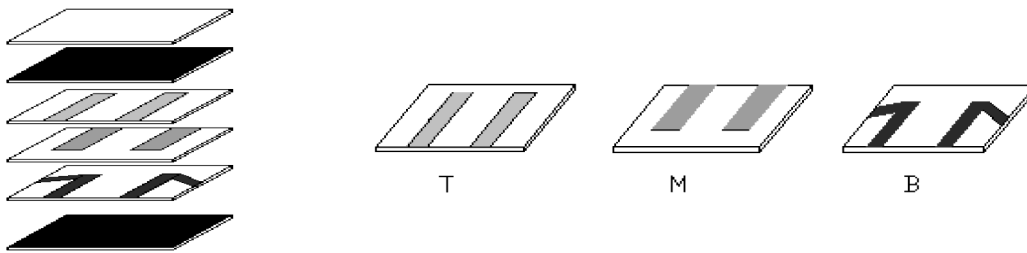


Figure 2: The structure of stripline configuration filter with LTCC.

The inductance matrix can be expressed as:

$$[L]_{n,m} = \epsilon_0\mu_0 [C_0]_{n,m}^{-1} \quad (5)$$

With the equations based on the multipolar method we can get the capacitance matrix and the inductance matrix. we have proved that the method is convincing.

3. Modified Equivalent Circuit of BPF (Bandpass Filter)

3.1. Analysis of the Striplines Configuration Filter [5–7]

The schematic configuration for the striplines filter to be implemented is shown in Figure 2. It is consisted by three layers: *T* layer, *M* layer, and *B* layer. It is shown that this is a two LC resonance filter, and the configuration of two LC resonance is uniform. In the experimental filter, inductance *L* of resonance is presented by self-in-inductance LM of conductor *M*. resonate capacitance *M* is presented by self-in-capacitance CM of conductor *M* and coupling capacitance CT between conductor *M* and conductor *T* and coupling capacitance CB between conductor *M* and conductor *B*. Coupling C12 between resonance cells are consisted by the total of each coupling capacitance.

We give the modified equivalent circuit about the striplines configuration filter, as shown in Figure 2. The schematic illustration of the modified equivalent circuit is shown as Figure 4:

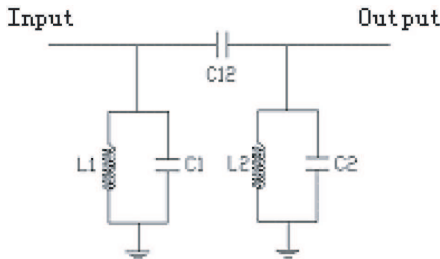


Figure 3: Traditional equivalent circuit.

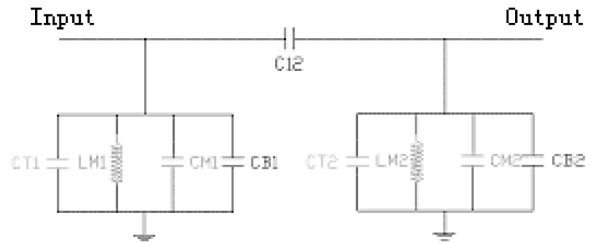


Figure 4: Modified equivalent circuit.

In traditional equivalent circuit, there is no one-to-one relationship between the striplines configuration and equivalent circuit numerical value in detail. But in modified equivalent circuit, there is one-to-one relationship between the striplines configuration and equivalent circuit numerical value in detail.

3.2. Simulation Results

The scattering parameter S_{11} , S_{21} can be expressed as follows:

$$IL = 10 \log \frac{P_{in}}{P_L} = 10 \log \frac{1}{|S_{21}|^2} = -10 \log |S_{21}|^2 \text{ (dB)} \tag{6}$$

where $S_{11} = \Gamma_{in}$, $\rho = \frac{1+|S_{11}|}{1-|S_{11}|}$, $\Gamma_{in} = \frac{Z_{in}-Z_0}{Z_{in}+Z_0}$

Every no-loss component can be expressed as:

$$|S_{21}|^2 = 1 - |S_{11}|^2 \tag{7}$$

Through the above parameters we can get Insert Loss (IL), Bandpass (B) and VSWR. The input impedance can be obtained in following equations:

$$Z_{in} = ((Z_L//Z_{CT2}//Z_{LM2}//Z_{CM2}//Z_{CB2}) + Z_{C12})//Z_{CT1}//Z_{LM1}//Z_{CM1}//Z_{CB1} \tag{8}$$

The characteristic parameter of the component can be expressed in curves through following equations:

$$S_{11} = 20 \log \left| \frac{Z_{in} - Z_G}{Z_{in} + Z_G} \right| \text{ (dB)} \tag{9}$$

$$S_{21} = 10 \log(1 - |S_{11}|^2) = 10 \log \left(1 - \left| \frac{Z_{in} - Z_G}{Z_{in} + Z_G} \right|^2 \right) \text{ (dB)} \tag{10}$$

Now we provide a multiplayer ceramic microwave filter with the size of 2.0 mm × 1.25 mm × 0.95 mm³ to certify the correctness of the method comparing HFSS simulation with the dielectric constant 27:

The following graphs demonstrate the results respectively:

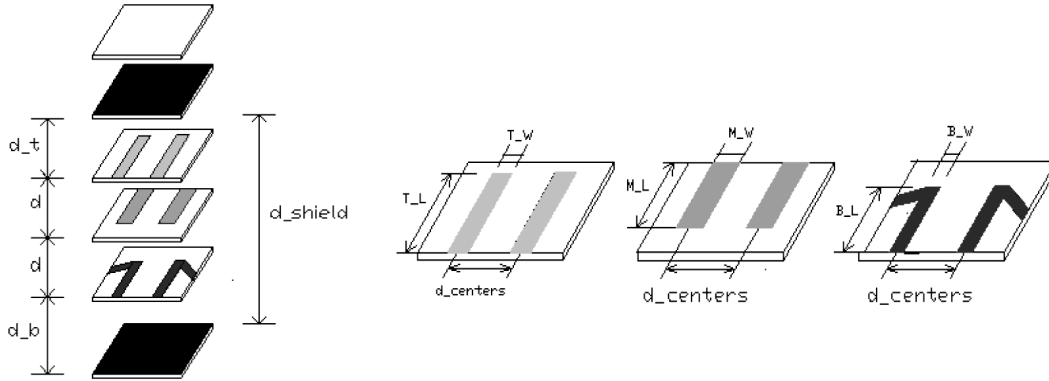


Figure 5: The structure of models.

Table 1: The models physical size is stated follow(unit: mm)

model	d1	d2	d3	d4	T_L	T_W	M_L	M_W	B_L	B_W
0	0.045	0.26	0.28	0.5	1	0.15	1	0.35	1	0.25
1	0.05	0.26	0.28	0.5	1	0.15	1	0.35	1	0.25
2	0.04	0.26	0.28	0.5	1	0.15	1	0.35	1	0.25
3	0.045	0.26	0.28	0.6	1	0.15	1	0.35	1	0.25
4	0.045	0.26	0.28	0.7	1	0.15	1	0.35	1	0.25
5	0.045	0.26	0.28	0.6	1	0.15	0.8	0.3	1	0.25
6	0.045	0.26	0.28	0.6	1	0.15	0.8	0.5	1	0.25
7	0.048	0.49	0.55	0.8	2.3	0.4	2.3	0.6	2.3	0.2
8	0.048	0.49	0.55	0.65	2	0.2	2	0.4	2	0.3
9	0.048	0.49	0.55	0.65	1	0.15	3	0.3	1	0.25

Note: d1=d,d2=d_t,d3=d_b,d4=d_centers

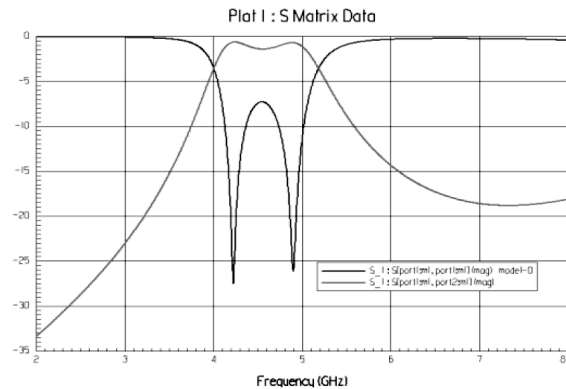
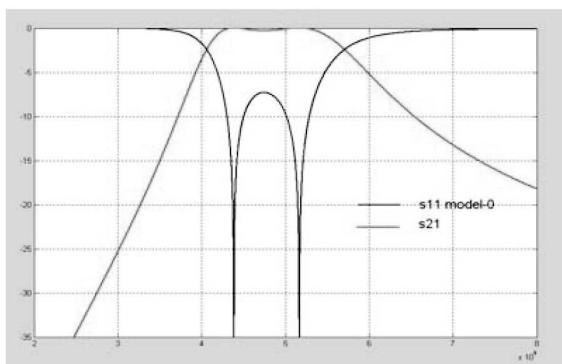


Figure 6: Result using the modified equivalent circuit(left) and with HFSS(right).

Analyzing the two graphs above, several differences can be found including inset loss, stop band attenuation, band width, reflection in the input port.

4. Conclusion

The simulation results prove that modified equivalent circuit model where the relationship between the concentrate parameters and physical dimension of LTCC microwave filter is corrected. The novel design method

of field-circuit has high efficiency, therefore, the designing time can be shortened.

Acknowledement

The authors would like to acknowledge Zhejiang Zheng Yuan Electric CO., Ltd. for provided materials for device fabrication.

REFERENCES

1. Ishizaki, T., T. Uwano, and H. Miyake, "An extended configuration of a stepped impedance comb-line filter," *IEICE Trans. Electron.*, E79-C, 671–678, 1996.
2. Sim, S. H., C. Y. Kang, S. J. Yoon, Y. J. Yoon, and H. J. Kim, "Broadband multilayer ceramic chip antenna for handsets," *Electron. Lett.*, Vol. 38, 205–207, 2002.
3. Lew, D. W., J. S. Park, D. Ahn, N. K. Kang, C. S. Yoo, and J. B. Lim, "A design of the ceramic chip balun using the multilayer configuration," *IEEE Trans. Microwave Theory Tech.*, Vol. 49, 220–224, 2001.
4. Dernovsek, O., A. Naeini, G. Preu, W. Wersing, M. Eberstein b, and W. A. Schiller, "LTCC glass-ceramic composites for microwave application," *Journal of the European Ceramic Society*, Vol. 21, 1693–169, 2001.
5. Leung, W. Y., K. Keung, M. Cheng, and K. L. Wu, "Multilayer LTCC bandpass filter design with enhanced stopband characteristics," *IEEE Microwave and Wireless Components Letters*, Vol. 12, No. 7, 240–242, 2002.
6. Sim, S. H., C. Y. Kang, and J. W. Choi, "A compact lumped-element lowpass filter using low temperature cofired ceramic technology," Vol. 23, 2717–2720, 2003.
7. Zhao, Y. J. and Y. Z. Yin, "An efficient design method of LTCC filters with aggressive space mapping technique," *Microwave and Optical Technology Letters*, Vol. 41, No. 1, 24–28, 2004.

Design of a Metafilm-composite Dielectric Shielding Structure Using a Genetic Algorithm

J. Y. Huang¹, M. Y. Koledintseva¹, P. C. Ravva¹, J. L. Drewniak¹
R. E. DuBroff¹, B. Archambeault², and K. N. Rozanov³

¹University of Missouri-Rolla, USA

²IBM Co., USA

³Russian Academy of Sciences, Russia

Abstract—An analytical model for a shielding structure containing both bulk composite layers and planar metafilms (MFs) made of perfect electric conductors is presented, allowing for synthesis of shielding structures using the genetic algorithm (GA) optimization. MFs can be of two different types: patch or aperture. The frequency response, specifically, transmission (T) and reflection (Γ) coefficients in a plane-wave formulation, of any MF is calculated based on polarizabilities determined by the particular pattern geometry. T and Γ of a patch-type MF are derived using the generalized sheet transition conditions (GSTC) and the Babinet's duality principle is used for aperture-type MF to map the results from the complementary problem. T and Γ for a single-layered MF are represented in a unified matrix form for any angle of incidence. T -matrix approach is used for getting T and Γ for a multilayered structure. Any MF buried in a host dielectric can be decomposed into three types of basic elements: a host composite slab, interface between media, and an MF inside the homogeneous host medium. Each basic element is described by a corresponding T -matrix, and the total T -matrix of the stack is the sequential product of the each individual T -matrix. T and Γ of the stack can be easily derived from the total T -matrix. If there are two or more MFs, the distance between them justifies the condition of neglecting higher-order evanescent mode interactions. Then the GA is applied to engineer a structure with the desired frequency response. It helps to choose the best geometry of MF patterns, thickness of layers, and appropriate constitutive parameters of each composite layer.

1. Introduction

For many practical applications, it is desirable to develop shielding structures having specified frequency characteristics. Application of a robust and quickly converging genetic algorithm (GA) facilitates the engineering of composite materials, saving time and resources before manufacturing and testing real materials [1]. A shielding structure may consist of a single composite dielectric or a multilayered stack of composite dielectrics with given electromagnetic properties. However, composite dielectric layers alone may be insufficient for achieving the acceptable shielding effectiveness (SE) in a given frequency range. The presence of metafilms (MFs) buried in composite layers may increase SE in the frequency band of interest, or assure desirable frequency-selective effects.

In this work, a model of a shielding structure containing both bulk composite layers and MFs made of PEC has been developed analytically, and the approach is considered below. For simplicity, we only consider MFs constructed by square arrays (with the same periodicity along two orthogonal axes in the plane) buried inside a homogeneous host material.

2. Mathematical Model

2.1. Using T-matrix Approach to Analyze T and Γ of the Multilayered Structures

The T -matrix used in this model is similar to that defined in [2]. A wave-transmission system is modeled as a two-port network. The forward and backward waves at the input and output ports are related as

$$\begin{bmatrix} a_1 \\ b_1 \end{bmatrix} = \begin{bmatrix} t_{11} & t_{12} \\ t_{21} & t_{22} \end{bmatrix} \cdot \begin{bmatrix} b_2 \\ a_2 \end{bmatrix}, \quad (1)$$

where a_1 and a_2 are the incoming wave and b_1 and b_2 are outgoing waves.

The total T -matrix of N cascaded 2-port networks T_1, T_2, \dots, T_N is the sequential product of the corresponding T -matrices,

$$T_{tot} = \begin{bmatrix} t_{11}^{tot} & t_{12}^{tot} \\ t_{21}^{tot} & t_{22}^{tot} \end{bmatrix} = T_1 T_2 \dots T_N. \quad (2)$$

Then T and Γ of the multilayered MF can be found as [2]:

$$T = t_{21}^{tot} = b_2/a_1 \big|_{a_2=0} \quad \text{and} \quad \Gamma = t_{11}^{tot} = b_1/a_1 \big|_{a_2=0}. \quad (3)$$

Any MF buried in a host medium can be decomposed into 3 basic elements: (a) a host medium slab; (b) a medium interface, and (c) an MF inside the homogeneous host medium, as shown in Fig. 1. T-matrices will be obtained below for all these three cases. Then T and Γ of the stack can be easily obtained from (2) and (3).

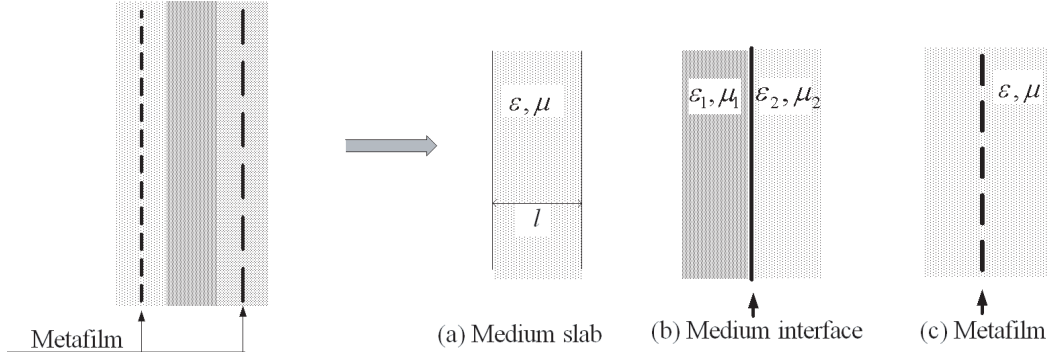


Figure 1: Decomposition of multilayered MF.

2.2. Formulation for a Composite Layer

The Maxwell Garnett (MG) effective medium formulation can serve as a basis for engineering composite microwave materials [1],

$$\varepsilon_{eff} = \varepsilon_b + \frac{\frac{1}{3} \sum_{i=1}^n f_i (\varepsilon_i - \varepsilon_b) \sum_{j=1}^3 \frac{\varepsilon_b}{\varepsilon_b + N_{ij} (\varepsilon_i - \varepsilon_b)}}{1 - \frac{1}{3} \sum_{i=1}^n f_i (\varepsilon_i - \varepsilon_b) \sum_{j=1}^3 \frac{N_{ij}}{\varepsilon_b + N_{ij} (\varepsilon_i - \varepsilon_b)}}, \quad (4)$$

where $\varepsilon_b(j\omega) = \varepsilon_{\infty b} + \chi_b(j\omega)$ and $\varepsilon_i(j\omega) = \varepsilon_{\infty i} + \chi_i(j\omega)$ are the relative permittivity of a base dielectric and of the i -th type of inclusions, respectively; $\varepsilon_{\infty b, i}$ are the high-frequency permittivities for the base material and inclusions of the i -th type, respectively; and $\chi_{b, j}(j\omega)$ are the corresponding dielectric susceptibility functions. f_i is the volume fraction occupied by the inclusions of the i -th type; N_{ij} are the depolarization factors of the i -th type of inclusions, and the index $j = 1, 2, 3$ corresponds to $x, y,$ and z Cartesian coordinates. The effective permittivity of a mixture might have complex-shaped frequency dependence. As shown in [1], it can be approximated by a series of Debye-like terms with real relaxation constants τ_k and complex (in general case) coefficients A_k . The coefficients A_k can be found using the genetic algorithm (GA) optimization technique [3],

$$\varepsilon_{eff}(j\omega) = \varepsilon_{\infty eff} + \chi_{eff}(j\omega) = \varepsilon_{\infty eff} + \sum_{k=1}^N \frac{A_k}{1 + j\omega\tau_k}. \quad (5)$$

The T -matrix of the homogenized composite slab with a thickness of l is as in [4]:

$$T_S = \begin{bmatrix} e^{jkl \cos \theta} & 0 \\ 0 & e^{-jkl \cos \theta} \end{bmatrix}, \quad (6)$$

where $k = \omega \sqrt{\varepsilon_{eff} \mu}$ is the wave number of the effective composite medium, and θ is the angle of incidence.

2.3. T-matrix for an Interface of Two Media

Let two media have permittivities $\varepsilon_1, \varepsilon_2$ and permeabilities μ_1, μ_2 , respectively. The T -matrix [4] is

$$T_I = \frac{1}{\tau_{T1}} \begin{bmatrix} 1 & \rho_{T1} \\ \rho_{T1} & 1 \end{bmatrix}, \quad (7)$$

where

$$\tau_{T1} = \frac{\eta_{T2} - \eta_{T1}}{\eta_{T2} + \eta_{T1}}, \quad \rho_{T1} = \frac{2\eta_{T2}}{\eta_{T2} + \eta_{T1}}, \quad \eta_{T1,2} = \begin{cases} \sqrt{\mu_{1,2}/\varepsilon_{1,2}} / \cos \theta & \text{for } TE \text{ plane wave;} \\ \sqrt{\mu_{1,2}/\varepsilon_{1,2}} \cdot \cos \theta & \text{for } TM \text{ plane wave.} \end{cases} \quad (8)$$

2.4. Plane Wave Formulas for Single-layered MFs

2.4.1. Extended GSTC for MFs

For an MF buried inside a homogeneous host medium with permittivity ε_{eff} and permeability μ , suppose the microscopic polarizability tensor $\bar{\bar{\alpha}}$ of the pattern is

$$\bar{\bar{\alpha}} = \begin{bmatrix} \bar{\bar{\alpha}}_{ee} & \bar{\bar{\alpha}}_{em} \\ \bar{\bar{\alpha}}_{me} & \bar{\bar{\alpha}}_{mm} \end{bmatrix}. \quad (9)$$

Extending the GSTC [5] for the case when there is cross-coupling between electric and magnetic polarizations of individual scatterers of MFs, the following boundary conditions for any metafilm in (xy) plane can be derived:

$$\begin{aligned} \hat{z} \times \vec{H} \Big|_{z=0^-}^{0^+} &= j\omega [\bar{\bar{\alpha}}_{EE,t} \quad \bar{\bar{\alpha}}_{EM,t}] \cdot \begin{bmatrix} \vec{E} \\ \vec{H} \end{bmatrix}_{av} - \hat{z} \times \nabla_t \left([\bar{\bar{\alpha}}_{ME,z} \quad \bar{\bar{\alpha}}_{MM,z}] \cdot \begin{bmatrix} \vec{E} \\ \vec{H} \end{bmatrix}_{av} \right); \\ \vec{E} \Big|_{z=0^-}^{0^+} \times \hat{z} &= -j\omega\mu [\bar{\bar{\alpha}}_{ME,t} \quad \bar{\bar{\alpha}}_{MM,t}] \cdot \begin{bmatrix} \vec{E} \\ \vec{H} \end{bmatrix}_{av} - \frac{1}{\varepsilon_{eff}} \nabla_t \left([\bar{\bar{\alpha}}_{EE,z} \quad \bar{\bar{\alpha}}_{EM,z}] \cdot \begin{bmatrix} \vec{E} \\ \vec{H} \end{bmatrix}_{av} \right) \times \hat{z}, \end{aligned} \quad (10)$$

where the tensors are sub-components of the macroscopic polarizability, determined by the microscopic polarizability $\bar{\bar{\alpha}}$ and periodicity of the metafilm pattern. Assuming that the pattern periods are equal, $D_x = D_y = D$,

$$\bar{\bar{\alpha}}^{mac} = \begin{bmatrix} \bar{\bar{\alpha}}_{EE} & \bar{\bar{\alpha}}_{EM} \\ \bar{\bar{\alpha}}_{ME} & \bar{\bar{\alpha}}_{MM} \end{bmatrix} = [D^2 \bar{\mathbf{I}} + \bar{\bar{\alpha}} \cdot \bar{\mathbf{G}}]^{-1} \cdot \bar{\bar{\alpha}}. \quad (11)$$

The matrix $\bar{\mathbf{G}} = \text{Diag} \left[-\frac{1}{4R\varepsilon_{eff}} \quad -\frac{1}{4R\varepsilon_{eff}} \quad \frac{1}{2R\varepsilon_{eff}} \quad -\frac{1}{4R} \quad -\frac{1}{4R} \quad \frac{1}{2R} \right]$, where $R \approx 0.6956D$, according to [5].

2.4.2. T and Γ for Single-layered Patch-type MFs at the Oblique Plane Wave Incidence

Consider the TE or TM plane waves as in Fig. 2.

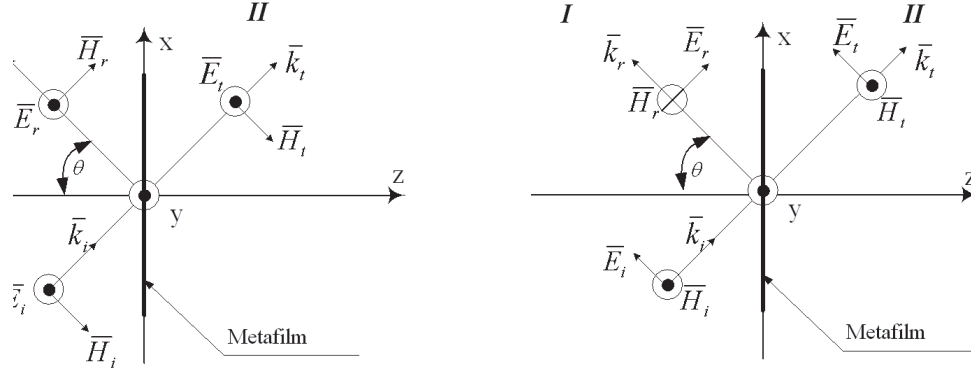


Figure 2: TE and TM polarized plane waves.

Using the GSTC and the approach in [6], let us introduce the forward and backward vectors $\bar{\mathbf{C}}_{TE(TM)}^+$ and $\bar{\mathbf{C}}_{TE(TM)}^-$ as

$$\bar{\mathbf{C}}_{TE}^{\pm} = [0 \quad 1 \quad 0 \quad \mp \cos\theta/\eta \quad 0 \quad \sin\theta/\eta]^T; \quad \bar{\mathbf{C}}_{TM}^{\pm} = [\cos\theta \quad 0 \quad \mp \sin\theta \quad 0 \quad \pm 1/\eta \quad 0]^T, \quad (12)$$

where $\eta = \sqrt{\varepsilon_{eff}/\mu}$.

The following linear system can be derived for solving $T_{TE(TM)}$ and $\Gamma_{TE(TM)}$:

$$\begin{bmatrix} A_{1,TE(TM)} & A_{2,TE(TM)} \\ 1 & -1 \end{bmatrix} \cdot \begin{bmatrix} T_{TE(TM)} \\ \Gamma_{TE(TM)} \end{bmatrix} = \begin{bmatrix} A_{3,TE(TM)} \\ 1 \end{bmatrix}, \quad (13)$$

$$\begin{aligned} A_{1,TE} &= ([U_{TE(TM)}] - [V_{TE}] \cdot \bar{\bar{\alpha}}^{mac}) \cdot \bar{\mathbf{C}}_{TE}^+; & A_{1,TM} &= ([U_{TM}] + [V_{TM}] \cdot \bar{\bar{\alpha}}^{mac}) \cdot \bar{\mathbf{C}}_{TE}^+; \\ A_{2,TE} &= -([U_{TE}] + [V_{TE}] \cdot \bar{\bar{\alpha}}^{mac}) \cdot \bar{\mathbf{C}}_{TE}^-; & A_{2,TM} &= (-[U_{TM}] + [V_{TM}] \cdot \bar{\bar{\alpha}}^{mac}) \cdot \bar{\mathbf{C}}_{TM}^-; \\ A_{3,TE} &= ([U_{TE}] + [V_{TE}] \cdot \bar{\bar{\alpha}}^{mac}) \cdot \bar{\mathbf{C}}_{TE}^+; & A_{3,TM} &= ([U_{TM}] - [V_{TM}] \cdot \bar{\bar{\alpha}}^{mac}) \cdot \bar{\mathbf{C}}_{TE}^+; \end{aligned} \quad (14)$$

where the elements $A_{i,TE(TM)}$ are

$$\begin{aligned} [U_{TE}] &= [0 \ 0 \ 0 \ 1 \ 0 \ 0]; & [V_{TE}] &= [0 \ jk/(2\varepsilon_{eff}) \ 0 \ 0 \ 0 \ jk \sin \theta/2]; \\ [U_{TM}] &= [0 \ 0 \ 0 \ 0 \ 1 \ 0]; & [V_{TM}] &= [j\omega/2 \ 0 \ 0 \ 0 \ 0 \ 0]. \end{aligned} \quad (15)$$

2.4.3. T and Γ for Single Layered Aperture-type MFs

It is found that T and Γ cannot be calculated by directly applying the corresponding polarizabilities to the GSTC. However, this obstacle can be bypassed by solving the corresponding patch-type complementary problem, and then, using Babinet's duality principle [7, 8], mapping the results into T and Γ of the aperture-type MFs [9]. The relations between T and Γ for two complementary arrays at oblique incidence are

$$T_{TE} = -\tilde{\Gamma}_{TM} \quad \text{and} \quad \Gamma_{TE} = -\tilde{T}_{TM}. \quad (16)$$

In (16), the tilde refers to the complementary structure.

T-matrix of a metafilm buried in a homogeneous host material is

$$T_{M_{TE(TM)}} = \frac{1}{T_{TE(TM)}} \begin{bmatrix} 1 & -\Gamma_{TE(TM)} \\ \Gamma_{TE(TM)} & T_{TE(TM)}^2 - \Gamma_{TE(TM)}^2 \end{bmatrix} \quad (17)$$

2.5. Requirement for Distance d between Neighboring MFs

The distance d between two neighboring MFs must be large enough for the evanescent modes to sufficiently decay and not interfere with the propagating mode. Given the ratio δ of the amplitude of the most intense high-order mode to the amplitude of the main propagating mode, the following inequality must fulfill:

$$\left| e^{jd(k - \sqrt{k^2 - (2\pi/D)^2})} \right| < \delta. \quad (18)$$

Numerous simulations have shown that the ratio $\delta < 10\%$ is sufficient for neglecting the higher-order modes.

3. Genetic Algorithm for Synthesis of MF-Composite Shielding

Before the synthesis process, a designer should have some initial information based on a particular application of the shielding under design. The requirements for the desired frequency response of the shielding structure should be known, and an appropriate number of composite layers and the total maximum thickness of the structure, as well as the reasonable ranges of electromagnetic parameters of layers for the initial search pool should be specified.

The synthesis algorithm determines thickness and frequency dependence of the effective parameters of each layer. The GA yields a "recipe" of physical parameters (appropriate base material, aspect ratio, concentration, and conductivity of inclusions) for composite layers. The designer chooses the best solution (parameters characterizing the frequency dependence for composites, pattern geometry for MFs, and the order of layer disposition) for approximating the desired frequency response. This latter selection is based on a range of practically available ingredients with realistic parameters. Thus, the codes developed for the design of shielding structures with the desired frequency characteristic combine the Maxwell Garnett effective medium mixing rule, the described above analytical formulation, and the GA optimization procedure.

4. Computation Results

Consider the three-layer structure with two MFs as in Fig. 3(a). The parameters are the following: the slab thickness is $d_1 + d_2 + d_3 = 5$ mm, the cell period is $D_1 = D_2 = 2$ mm, the radius of the apertures in the left metafilm is $r_1 = 0.6$ mm, and the radius of the discs (or apertures) in the right metafilm is $r_2 = 0.6$ mm. The host dielectric is a composite containing carbon particles in a Teflon base $\varepsilon_b = 2.2$ (dispersion and loss are neglected). Carbon particles having conductivity of $\sigma = 1000$ S/m are shaped as cylinders with the aspect ratio $a = \text{length}/\text{diam} = 50$. Their volume fraction in the composite is 8%, while percolation threshold is higher than 9%. The best parameters of the composite from a shielding effectiveness point of view, and at the same time, practically available composite material components were chosen using the GA. The frequency characteristic of the composite dielectric with $\varepsilon_1(f)$ and $\mu_1 = \mu_0$ shown in Fig. 3(b) was modeled using (4) and approximated by one Debye term in (5). Fig. 3(c) shows the calculated transmission coefficient for the structure at different distances $d_{1,2,3}$. The best shielding effectiveness of the structure in the frequency range of interest is obtained

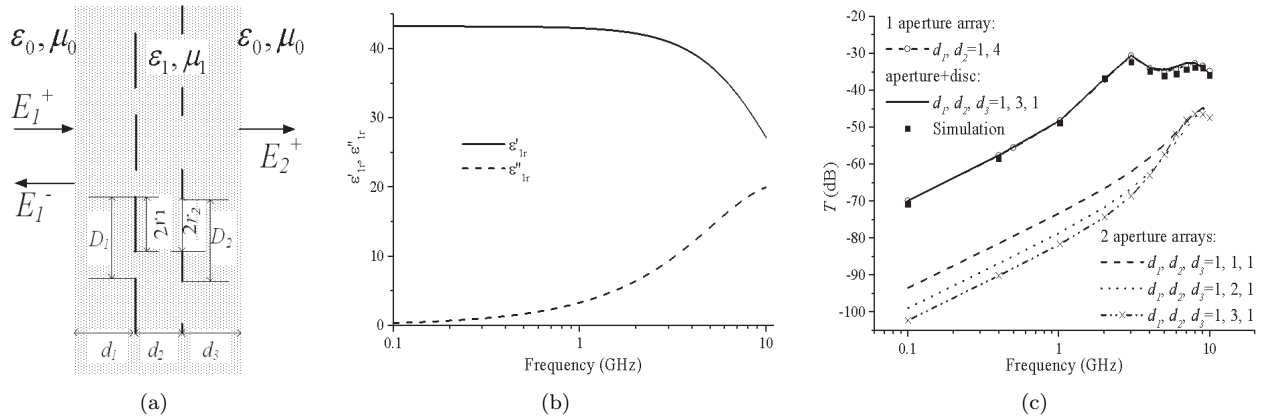


Figure 3: Multilayered structure with two different MFs buried in the composite dielectric layer.

with the thicknesses $d_1 = 1$ mm; $d_2 = 3$ mm; $d_3 = 1$ mm determined by the GA with two aperture MFs. Analytical and numerical simulation (using HFSS software) confirm this.

5. Conclusions

The shielding structures containing MFs and composite dielectrics can be engineered based on the presented analytical formulas for T and I and using an optimization GA. T and I are directly related to geometries of MF patterns, constitutive parameters, concentrations, and geometries of composite material phases. This approach provides a straightforward synthesis process for desirable frequency responses.

The effective parameters of the composites are modeled by Maxwell Garnett mixing formalism. The analytical formulas for T and I of multilayered MF structures are obtained using (1) the generalized GSTC, (2) the Babinet’s duality principle for complementary structures—aperture-type and patch-type MFs, and (3) the T -matrix cascading.

The analytical approach in this paper has an advantage over the full-wave numerical methods, since it saves computational resources for the synthesis process, and reduces the design cost prior to manufacturing.

REFERENCES

1. Koledintseva, M. Y., P. C. Ravva, R. E. DuBroff, J. L. Drewniak, K. N. Rozanov, and B. Archambeault, “Engineering of composite media for shields at microwave frequencies,” *Proc. IEEE EMC Symposium*, Vol. 1, 169–174, IL, Chicago, August 2005.
2. Collin, R. E., *Field Theory of Guided Waves*, 2nded. IEEE Press, New York, 1991.
3. Koledintseva, M. Y., J. Wu, J. Zhang, J. L. Drewniak, and K. N. Rozanov, “Representation of permittivity for multi-phase dielectric mixtures in FDTD modeling,” *Proc. IEEE Symp. Electromag. Compat.*, Vol. 1, 309–314, 2004, Santa Clara, CA, 9–13 Aug. 2004.
4. Orfanidis, S. J., *Electromagnetic Waves and Antennas*, <http://www.ece.rutgers.edu/orfanidi/ewa/>.
5. Kuester, E. F., M. A. Mohamed, M. Piket-May, and C. L. Holloway, “Averaged transition conditions for electromagnetic fields at a metafilm,” *IEEE Trans. Antennas Propagat.*, Vol. AP-51, 2641–2651, Oct. 2003.
6. Holloway, C. L., M. A. Mohamed, and E. F. Kuester, “Reflection and transmission properties of a metafilm with application to a controllable surface composed of resonant particles,” *IEEE Trans. Electromagn. Compat.*, Vol. EMC-47, 1–13, Oct. 2005.
7. Kong, J. A., *Electromagnetic Wave Theory*, 2nded. Wiley, New York, 1990.
8. Jackson, J. D., *Classical Electrodynamics*, 3rded. Wiley, New York, 1999.
9. Lee, S. W., G. Zarrillo, and C. L. Law, “Simple formulas for transmission through periodic metal grids or plates,” *IEEE Trans. Antennas Propagat.*, Vol. AP-30, 904–909, Sep. 1982.

Towards Nano-scales in Photonics

M. Soljačić, A. Karalis, E. Lidorikis, and M. Ibanescu
MIT, USA

L. V. Hau
Harvard University, USA

J. D. Joannopoulos
MIT, USA

We will discuss possible solutions to several key fundamental problems in nanophotonics. The goal of nanophotonics is to explore and manipulate photons at scales (in space, time and energy) that are orders of magnitude smaller than anything previously possible. To accomplish this, one needs to constrain visible or near-infrared photons (the preferred mode of operation: $\lambda \sim 1 \mu\text{m}$) into scales compatible with nanotechnology: 10–100 nm. One also needs to drastically reduce the operational power of optical devices, eventually even down to single photon operating energies.

Most of these problems could be tackled by Surface Plasmon (SP) based devices. SPs enable constraining, and manipulation of light at scales compatible with nanophotonics. Unfortunately, SP-supported designs suffer from two other major disadvantages: huge losses (characteristic of plasmonic materials), and small bandwidth (since SPs are resonance-supported phenomena). We will present a novel class of surface plasmon (SP) assisted components that can overcome all of these difficulties. We will show results of a detailed theoretical and numerical study of the underlying physical mechanism driving these novel SP components.

For a long time, there was a widespread belief in the optics community that alloptical signal processing is not feasible because of the weakness of ultra-fast non-linear effects. There are two most commonly used approaches to enhance non-linear effects. One is to use a material that has as large a non-linear response as possible. The other approach involves finding a structure whose geometrical properties optimize non-linear response. As far as materials go, Electro-Magnetically Induced Transparency (EIT) materials have by far the strongest non-linear response in nature: Kerr non-linearities 12 orders of magnitude larger than in GaAs have been measured in EIT systems recently, thus making EIT-materials the most non-linear materials in nature. Concerning the structural enhancement of non-linearities, Photonic Crystal (PhC) micro-cavities are superior to all other proposed systems: one can design tiny ($O(\lambda^3)$), low operational power (e.g., few tens of mW), ultra-fast (bit rate ≥ 40 Gbit/sec) devices suitable for any kind of all-optical signal processing, that can be implemented in common optical materials (AlGaAs, As₂Se₃...). We will present a detailed theoretical and numerical investigation of the possibility of combining the unparalleled non-linear properties of EIT materials, with superb opportunities of PhC micro-cavities for structural enhancement of non-linear effects in order to produce an all-optical non-linear device that can be operated at extraordinarily low (even single photon) energy levels.

Design and Measurement of a Four-port Device Using Left-handed Metamaterials

Z. M. Thomas, T. M. Grzegorzcyk, B.-I. Wu, X. D. Chen, and J. A. Kong
Massachusetts Institute of Technology, USA

A left-handed metamaterial can be designed such that the frequency dispersive nature of the constitutive parameters results in a change in the sign of refraction with frequency for a specified incidence angle [1]. A four-port device is designed that utilizes this property and reflection to separate an signal incident from port 1, into three distinct bandwidths. Power transmitted at the metamaterial interface is later collected at a port corresponding to either positive or negative refraction accordingly (ports 3 and 4). Power in the band of frequencies where the dominant effect is reflection is collected at a third output port (port 2).

Designing the device requires the selecting of an appropriate metamaterial that will support negative refraction in some bandwidth, and positive refraction in another. The incidence angle should be selected such that these properties can be realized, and a third band exists where reflection is dominant. Because the energy transmitted into the metamaterial must also exit the metamaterial before being detected at either of the two transmission ports, the geometry affecting the exit angle must also be considered and specified. Ideally the transmitted power exits the metamaterial with minimal internal reflection and is directed directly towards the appropriate port.

We present a design of the four-port device that utilizes the split-ring resonators introduced in [2]. This structure can achieve a Lorentz type dispersion relation [3]. The rings are all oriented in the same direction resulting in dispersion in one component of the permeability tensor. The ring design dimensions are supplied from [4] and the dispersive behavior is verified by simulation followed by applying the retrieval algorithm in [5]. After investigating and specifying the design parameters we find that a wedge of the material can be fashioned to achieve the desired properties. The device is constructed for measurements inside a parallel plate waveguide. Measurements are taken at the edge of a parallel plates utilizing SMA to X-band waveguide adapters. The X-band corresponds to the resonance region of the split-ring resonators. Measurements are made on a vector network analyzer and are found to be consistent with analytical expectations.

REFERENCES

1. Smith, D. R. and D. Schurig, "Electromagnetic wave propagation in media with indefinite permittivity and permeability tensors," *Phys. Rev. Lett.*, Vol. 90, No. 7, 077405, February 2003.
2. O'Brien, S. and J. B. Pendry, "Magnetic activity at infrared frequencies in structured metallic photonic crystals," *J. Phys.: Condens. Matter*, 6383–6394, June 2002.
3. Shelby, R. A., D. R. Smith, and S. Schultz, "Experimental verification of a negative index of refraction," *Science*, Vol. 292, 77–79, April 2001.
4. Wang, W., "Directive antenna using metamaterial substrates," *MIT Masters Thesis*, June 2004.
5. Chen, X., T. M. Grzegorzcyk, B.-I. Wu, J. P. Jr., and J. A. Kong, "Improved method to retrieve the constitutive effective parameters of metamaterials," *Phys. Rev. E*, Vol. 70, No. 016608, 1–7, 2004.

Embedded-circuit Meta-materials for Surface Wave Suppression

H. Mosallaei

Northeastern University, USA

Suppressing surface waves is a very challenging task in electromagnetics. Many researchers have proposed different configurations to stop the surface wave propagation. One of the most efficient ways has been based on the use of periodic dielectric and metallo-dielectric Electromagnetic Band-Gap (EBG) structures [1–2]. However, the periodicity of such structures is comparable to the wavelength and at least a few periods are required to achieve high isolation which is not very appropriate in the design of small size devices and systems.

In this paper a novel approach based on negative μ materials for suppressing the surface waves is offered. To accomplish this, Embedded-Circuit Loops (ECL), realizing artificial molecules, are printed on a low dielectric material. For a magnetic excitation polarized along the axis of the loops, the designed meta-material presents negative permeability property. In the negative μ region, the wave is stopped and cannot penetrate through the material [3]. Unlike traditional EBGs the periodicity of ECL can be a very small fraction of a wavelength ($< 0.05\lambda$). Fig. 1(a) depicts the geometry of a 1-layer ECM. The transmission coefficient for a plane wave illuminating a very thin layer of a ECM is shown in Fig. 1(b). The stop-band behavior is clearly demonstrated.

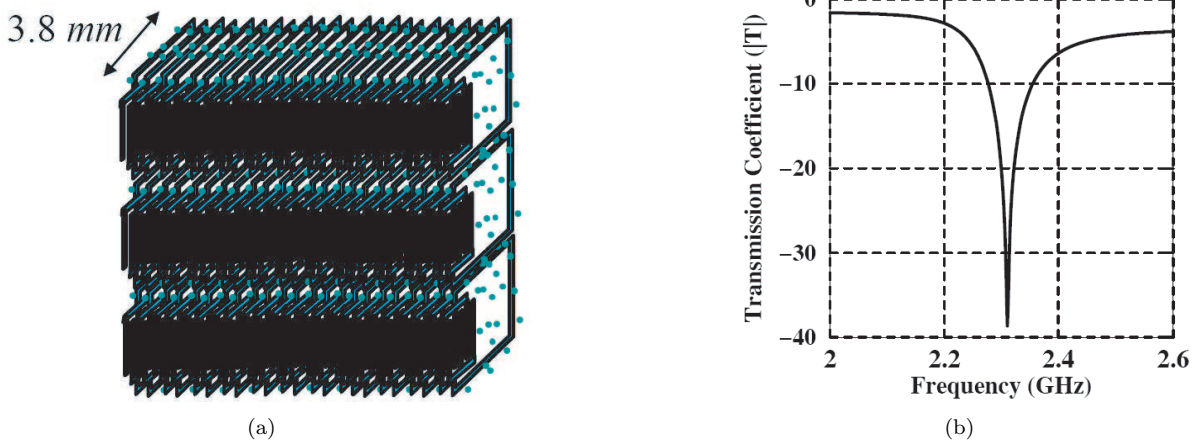


Figure 1: (a) Embedded-Circuit Metamaterial and (b) its performance.

REFERENCES

1. Rahmat-Samii, Y. and H. Mosallaei, "Electromagnetic band-gap structures: classification, characterization, and applications," *IEE International Conference on Antennas and Propagation*, UMIST, Manchester, UK, 2001.
2. Yang, F. and Y. Rahmat-Samii, *IEEE Trans. Antennas Propagat.*, Vol. 51, No. 10, 2936–2946, Oct. 2003.
3. Sarabandi, K. and H. Mosallaei, "Novel artificial embedded circuit meta-material for design of tunable electro-ferromagnetic permeability medium," *IEEE International Microwave Symposium*, Philadelphia, Pennsylvania, 2003.

Double Clad Fiber Laser with Frequency Selecting by Double Clad Fiber Bragg Grating

T. Wu¹ and Z.-D. Xue²

¹LongYan University, China

²Fuzhou University, China

It is always using F-P linearity cavity in double clad fiber lasers. The cavity is composed of one dichroic mirror and fiber end Fresnel reflector (reflectivity nearly 4%). This is a defect and unstable cavity. It cannot exactly select frequency, and the line width of the laser is extensive. In some applications requiring wavelength strictly, this kind of laser is limited. As a rule Bragg gratings that compose a laser cavity are fabricated in a high germanosilicate host fiber and then spliced with an Yb³⁺-doped active fiber. Difference of parameters of the two kinds of fibers leads to additional losses of both pump and signal. A double-clad fiber Bragg grating which was fabricated in the core of Yb³⁺-doped double-clad fiber using the phase-mask method is reported. This kind of grating is used as the output mirror of the D-shape inner cladding Yb³⁺-doped double-clad fiber laser. The fiber length is 10 m and 20 m respectively. The laser operating near 1058 nm with stable and narrow FWHM (3 dB bandwidth is 0.329 nm) is realized. The maximum output power laser is 570 mW. Finally, these experimental results are analyzed theoretically. A double clad fiber Bragg grating remarkably greatly improves the Spectrum properties of laser, and the anticipative wavelength of laser can be achieved. For the splice loss in cavity of the DCFL is very little, the bulk of the DCFL is reduced. It is also shown that wavelength-definite, narrow linewidth, high-efficiency, high-beam-quality laser performances can be achieved, which are of great interest for many important applications.

Ferroelectric PSTO and Mn: BSTO Thin Films for Wireless Microwave Elements

Z. Yuan¹, S. W. Liu², and C. L. Chen¹

¹University of Texas at San Antonio, USA

²University of Arkansas, USA

Ferroelectric thin films have broad applications in electronic, optoelectronic, optical, acoustic and microwave devices areas. Especially, there has been a significant increasing need of films in wireless microwave communications, such as microwave phase shifters, filters, and oscillators. Currently, ferroelectric BSTO and PSTO thin films are considered to be very promising candidates for room temperature tunable microwave elements because of their high dielectric tunability and relative low dielectric loss.

Recently, we have focused on the improvement of dielectric properties of the highly epitaxial ferroelectric thin films. A novel method of 2% Mn additional-doping technique was adapted to the pure BSTO/MgO films. The as-growth films were characterized by x-ray diffraction and transmission electron microscopy to understand the microstructure, crystallinity, epitaxy behaviors. The microstructural studies reveal that both BSTO and PBCO thin films are c-axis oriented with excellent single crystalline and excellent epitaxial behavior although both BSTO and PBCO film have large lattice mismatch with (001)MgO substrate at about 6% and 7.5%, respectively. The epitaxial relationships were found to be $(001)_{\text{films}} // (001)_{\text{MgO}}$ and $[100]_{\text{film}} // [100]_{\text{MgO}}$.

To understand the dielectric properties of the as-grown PSTO and Mn:BSTO films, high frequency dielectric measurements were employed to analyze the dielectric properties of Mn: BSTO and PSTO thin films. A significant improvement of dielectric property of the as-grown Mn: BSTO films was achieved with large tenability of 80% at 40 KV/cm, very large dielectric constant value of 3800 and extra low dielectric loss of only 0.001 at 1 MHz measuring frequency and room temperature. The mechanisms responsible for this improvement concern the fact that the acceptor dopants Mn^{2+} can compensate for the electrons generated from the oxygen vacancies, whose hopping between different titanium ions will induce the dielectric loss. The high frequency (10-30 GHz) dielectric measurements demonstrate that the Mn: BSTO films are excellent in both dielectric property and very low insertion loss values of only 0.2 dB at 10 GHz and more than 1.5 dB at 30 GHz. On the other hand, the high frequency dielectric property measurements on the as-grown PSTO/MgO thin films exhibit a high dielectric constant value of 1420 at zero-bias and a very large tunability at 34% under bias field 40 Kv/cm up to 20 GHz. In summary, these results indicate that highly epitaxial Mn: BSTO and PSTO thin films are good candidates for developing the high-frequency, room-temperature tunable microwave.

Chain of Metamaterial Nanospheres as Leaky-wave Nanoantennas at Optical Frequencies

A. Alù^{1,2} and N. Engheta¹

¹University of Pennsylvania, USA

²University of Roma Tre, Italy

The theory for designing a traveling-wave or a leaky-wave antenna is well established at microwave frequencies. At these frequencies usually a waveguide structure with some radiating defects or corrugations periodically arranged in space can produce a guided beam that leaks some energy into free space. Under proper conditions on the periodicity and the guidance of the energy, this may produce a directive beam with potential applications in several fields. The advent of metamaterials, i.e., artificially engineered materials with unconventional properties not common in nature, has raised new interest in different areas including the leaky-wave antenna design. In particular, a proper design of planar metamaterial circuit boards has been shown by others to produce a compact leaky-wave antenna with interesting performance, in terms of the possibility of scanning the angle of radiation from end-fire to back-fire by varying the frequency of operation, without any cut-off at broadside [1, 2].

Extending these concepts to the optical frequencies can offer exciting possibilities and useful applications. However, such extension does not only involve the scale reduction, since materials (e.g., noble metals) behave differently in different frequency regimes. The recent interest in plasmonic resonances and related phenomena, however, has raised the attention on a possible new paradigm for extending the circuit concepts from lower frequencies into the visible domain. We have shown in [3] how nanocircuit elements can be envisioned at these frequencies and how they can be properly connected in order to synthesize a complex nanocircuit. In [4] we have followed this analogy to consider optical nano-transmission-lines by properly arranging nanoinductors and nanocapacitors. Following the same analogy, and exploiting linear chains of plasmonic particles interleaved with non-plasmonic gaps, here we show theoretically how it is possible to design highly directive leaky-wave antennas at optical frequencies with future potentials in communications and nanotechnology. A different way of designing leaky-wave antennas using periodically modulated epsilon-negative nanorods has recently been studied theoretically [5]

In the present work, we show the conditions on the plasmonic particles composition and on the geometrical properties of the chain for supporting such resonant modes and consequently for building directive nanoantennas at optical frequencies. We also propose some design examples and we verify the results with full-wave simulations utilizing realistic materials (e.g., silver) with dispersive properties and ohmic losses included.

REFERENCES

1. Grbic, A. and G. V. Eleftheriades, *IEEE Trans. Antennas Propagat.*, Vol. 50, 1494, 2002.
2. Lim, S., C. Caloz, and T. Itoh, *IEEE Microwave & Wireless Components Lett.*, Vol. 14, 277, 2004.
3. Engheta, N., A. Salandrino, and A. Alù, *PRL*, Vol. 95, 095504, 2005.
4. Alù, A. and N. Engheta, *Proc. of URSI GA*, New Delhi, India, Paper No. 99, 2005.
5. Li, J. and N. Engheta, "2005 annual meeting of the optical society of america," *Frontiers in Optics*, Tucson, Arizona, October 16-20, 2005.

Epsilon-near-zero (ENZ) Materials as Insulators for Nanocircuit Elements

M. G. Silveirinha^{1,2} and N. Engheta¹

¹University of Pennsylvania, USA

²Universidade de Coimbra, Portugal

There has been a growing interest in research on metamaterials with negative parameters, i.e., double-negative (DNG) or single-negative media [1, 2]. However, metamaterials with other unconventional material parameters have also attracted a great deal of attention. One class of such materials is the media in which the relative permittivity and or permeability is near zero. These materials, which can be referred to as epsilon-near-zero (ENZ) or mu-near-zero (MNZ), have been the subject of study recently [3, 4]. We have shown theoretically that electromagnetic or optical waves may be able to tunnel through very narrow channels or waveguide bends filled with ENZ materials, and that this property can play an interesting role in reducing the reflectivity at certain waveguide bends. It has also been shown that zero-index materials can be used to narrow the far-field pattern of an antenna embedded in the medium and to transform curved wavefronts into planar ones.

In the present work, we explore another interesting feature of ENZ materials, namely, their role as insulators for nano-scale circuit elements at the infrared (IR) and visible frequencies. The concept of circuit elements in the optical domains, i.e., nanoinductors, nanocapacitors, and nanoresistors has been introduced recently [5], in which it was suggested that plasmonic and non-plasmonic nanoparticles can behave as circuit elements, i.e., inductor and capacitor, at optical frequencies. One of the interesting questions in this context is the following: “Can we have an equivalent of “insulators” or “shields” for such nanocircuit elements at the optical frequencies that minimizes the coupling between the circuit elements?”. One possible answer to this question is the use of ENZ layers as insulating shields around optical nanoelements. Our theoretical analysis has shown that such layers can, under certain circumstances, indeed act as insulators supporting zero displacement current, resulting in the confinement of the displacement current inside the nanoparticles. Therefore, ENZ-shielded nanocircuit elements can be regarded as elements with lesser leakage coupling among neighboring nanoelements.

In this talk, we will present some of our theoretical results, and we will forecast some future ideas and potential applications for this concept.

REFERENCES

1. Ziolkowski, R. W. and N. Engheta (Guest editors), Special issue of *IEEE Transactions on Antennas and Propagation on metamaterials*, Vol. 51, No. 10, October 2003.
2. Itoh, T. and A. A. Oliner (Guest Editors), Special issue of *IEEE Transactions on Microwave Theory and Techniques*, Vol. 53, No. 4, April 2005.
3. Engheta, N., M. Silveirinha, A. Alù, and A. Salandrino, “Scattering and reflection properties of low-epsilon metamaterial shells and bends,” *2005 International Conference in Electromagnetics in Advanced Applications*, Turino, Italy, September 12–16, 2005.
4. Ziolkowski, R. W., “Propagation in and scattering from a matched metamaterial having a zero index of refraction,” *Physical Review E*, Vol. 70, 046608, 2004.
5. Engheta, N., A. Salandrino, and A. Alù, *Physical Review Letters*, Vol. 95, 095504, August 2005.

Leaky-mode Resonance Properties of Periodic Lattices and Their Applications

R. Magnusson and Y. Ding
University of Connecticut, USA

Subwavelength periodic photonic crystal slabs and waveguide gratings exhibit strong resonance effects. For periodic elements with weak dielectric-constant contrast, strong surface-localized fields with high Q-factors are found. As the modulation amplitude increases, the Q-factor falls and the resonant spectra broaden. These guided-mode resonance effects arise when an incident electromagnetic wave is coupled by a second-order grating to a leaky waveguide mode supported by the thin-film system. Such resonance effects can be applied to implement new photonic devices. For example, optical reflection (bandstop) filters with narrow spectral linewidths can be realized since the coupling of the external wave into the leaky, reradiated mode occurs over narrow parametric ranges. Resonant bandstop optical filters with high efficiencies ($\sim 98\%$) and narrow lines (~ 1 nm) have been experimentally verified in the near-IR spectral region. New resonant biosensors can be developed based on these concepts.

This paper provides analytical, numerical, and experimental results elucidating the nature of resonant leaky modes associated with periodic refractive-index lattices. It is shown by numerous simulations that single-layer subwavelength periodic leaky-mode waveguide films with binary profiles can be applied to fashion optical elements that provide a remarkably broad variety of spectral characteristics. These sparse elements even with one-dimensional periodicity can function as new types of narrow-line bandpass filters, polarized wideband reflectors, polarizers, polarization-independent elements, and as wideband antireflectors. The work presented addresses fundamental phenomena essential for development of subwavelength leaky-mode resonant device technologies. The associated physical properties are explained in terms of the photonic band structure and its relation to the structural symmetry of the elements. The interaction dynamics of the leaky modes at resonance contribute to sculpting the diverse spectral bands observed by numerical simulations. The leaky-mode spectral placement, their spectral density, and their levels of interaction are shown to be fundamentally important in understanding device operation. These results demonstrate potentially new dimensions in optical device design and may provide complementary capability with thin-film optics.

In addition to applications in the photonic band, it is of interest to consider applicability of guided-mode resonance effects in lower frequency spectral regions. For example, devices operating in the THz region are potential candidates. Thus, computed results are presented to illustrate key properties of resonant THz elements such as spectral profiles and resonance efficiencies with respect to the structural parameters defining the device.

Slow-than-light Transportation of Microwave through Subwavelength Fractal Slots

B. Hou, W. J. Wen, and P. Sheng

The Hong Kong University of Science and Technology, China

Recently, we have found that high electromagnetic wave transmissions can be achieved for a metal plate perforated by slots arranged in fractal geometry at wavelengths much larger than the cross sectional dimensions of fractal slots, and that the transmission is independent on the incident angle, plate thickness, or array periodicity [1,2]. Now, we investigate the wave transportation in time domain through the subwavelength fractal slots at the transmission peak. Both experimental and theoretical results reveal a slow-than-light phenomenon. For example, the time delay can reach 1.3 ns for a microwave pulse to propagate through a 7.7 mm thick metal plate with the fractal slots, which means a reduced group velocity of $c/50$. The time delay or the reduction in group velocity for a metal plate of thickness given is determined solely by the geometric of fractal slots, because the transmission is caused by a subwavelength resonance which is the transversal shape resonance localized in the metallic slots with axial wave number $k = 0$. The time delay can also be tuned by filling dielectrics into the fractal slots where the fields undergo a significant enhancement.

REFERENCES

1. Zhou, L., W. Wen, C. T. Chan, and P. Sheng, "Mechanisms for high electromagnetic wave transmissions," *PIERS 2005*, Hangzhou, China, 2005.
2. Wen, W., L. Zhou, B. Hou, C. T. Chan, and P. Sheng, "Microwave resonant transmission through sub-wavelength fractal slots," to be published.